Available online at www.sciencedirect.com
SCIENCE DIRECT®
Journal of Power Sources 124 (2003) 453–458
JOURNAL OF POWER SOURCES
www.elsevier.com/locate/jpowsour

Radiation heat transfer analysis of the monolith type solid oxide fuel cell

Sunil Murthy, Andrei G. Fedorov*

Woodruff School of Mechanical Engineering, Georgia Institute of Technology, Atlanta, GA 30332-0405, USA

Received 19 May 2003; accepted 12 June 2003

Abstract

In this study, a modeling framework for heat and mass transport is established for a unit monolith type SOFC, with emphasis on quantifying the radiation heat transfer effects. The Schuster–Schwartzchild two-flux approximation is used for treating thermal radiation transport in the optically thin yttria-stabilized-zirconia (YSZ) electrolyte, and the Rosseland radiative thermal conductivity is used to account for radiation effects in the optically thick Ni–YSZ and LSM electrodes. The thermal radiation heat transfer is coupled to the overall energy conservation equations through the divergence of the local radiative flux. Commercially available FLUENT^{TM} CFD software was used as a platform for the global thermal-fluid modeling of the SOFC and the radiation models were implemented through the user-defined functions. Results from sample calculations show significant changes in the operating temperatures and parameters of the SOFC with the inclusion of radiation effects.

Keywords: Thermal-fluid modeling; Solid oxide fuel cells; Radiative heat transfer

1. Introduction

Solid oxide fuel cells (SOFCs) are promising energy source under currently active development due to their high efficiency, high energy density and low emission of pollutants to the environment. SOFCs belong to the category of high temperature fuel cells and usually operate around 800–1000 °C. The high temperature operation allows for the use of natural gas as fuel, thereby eliminating the need for an expensive reformer system. Unfortunately, the high temperature also makes the fuel cell susceptible to many materials related modes of thermo-mechanical failure. Recently, mathematical modeling has been explored as a vital tool in the development and reliability prediction of fuel cells. An accurate modeling of the heat transfer mechanisms in the fuel cell is a prerequisite to developing reliable failure predictions tools.

Simplistic thermal models of fuel cells, using heat transfer correlations for assumed fluid flow configurations, have been carried out in the past [1]. More recently, temperature distributions in three-dimensional models of planar SOFC have been achieved by coupling the electrochemical effects with the solution of the Navier–Stokes equations of motion and energy/mass conservation [2].

Most existing models neglect the effect of radiation heat transfer. Yakabe et al. [3] found that inclusion of radiation heat exchange within the flow channels resulted in a flatter distribution of the temperature profile along the fuel cell. However, the above model neglects absorption, emission or scattering in the media and only accounts for the surface-to-surface radiation effects in the analysis. Though, Hartvigsen et al. [4] were able to demonstrate significant changes in stack temperature with the inclusion of radiation effects, not much detail was provided in terms of the properties used and the specific radiation model employed.

In the present study, the effect of radiative heat transfer on the fuel cell performance is reported. A single unit, monolith type, co-flow fuel cell (Fig. 1) model was studied by analyzing the fluid flow, species transport and conjugate heat transfer within the cell. The radiative heat transfer (RTE) equation was used to model radiation heat transfer and was solved using the discrete ordinate (DO) method. Alternately, a simplified radiation model was also developed based on the Schuster–Schwartzchild two-flux approximation and its accuracy was compared to that of the computationally expensive DO scheme.

* Corresponding author. Tel.: +1-404-385-1356; fax: +1-404-894-8496.
E-mail address: andrei.fedorov@me.gatech.edu (A.G. Fedorov).

0378-7753/$ – see front matter © 2003 Elsevier B.V. All rights reserved.
doi:10.1016/S0378-7753(03)00732-8

Nomenclature

c_0	speed of light in vacuum (m/s)
G	Gibb's free energy (J)
h	Planck's constant (J s)
H	reaction enthalpy (J)
k	Boltzmann constant (J/K)
k_R	Rosseland thermal conductivity (W/(m K))
n	refractive index of the medium
q_R	radiative heat flux (W/m^2)
T	absolute temperature (K)
Tr	transmittance

Greek letters

β_R	Rosseland-mean extinction coefficient (m^{-1})
κ	absorption coefficient (m^{-1})
λ	wavelength (μm)
σ	Stefan–Boltzmann constant (J/(K^4 m^2 s))
τ	optical thickness

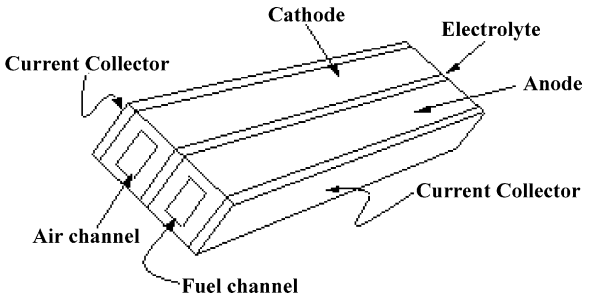

Fig. 1. Schematic of the monolith type fuel cell modeled.

2. Modeling methodology

2.1. Radiative properties

The prediction of radiation heat transfer in semi-transparent materials requires the knowledge of radiative properties, namely, the absorption coefficient and the scattering coefficient of the material. The state-of-the-art SOFCs uses yttria-stabilized-zirconia (YSZ) as the electrolyte, strontium-doped $LaMnO_3$ (LSM) as the cathode and nickel doped YSZ as the anode. The radiative properties of a material are usually a function of wavelength, and the spectral region of interest for thermal radiation can be obtained from the Planck's law for blackbody emissive power,

$$E_{b\lambda} = \frac{2\pi h c_0^2}{n^2 \lambda^5 [e^{hc_0/n\lambda kt} - 1]} \quad (1)$$

where $E_{b\lambda}$ is the spectral emissive power of a black body, h the Planck constant, c_0 the speed of light in vacuum, k the Boltzmann's constant, T the temperature and n the refractive index of the medium. The variation of the black body

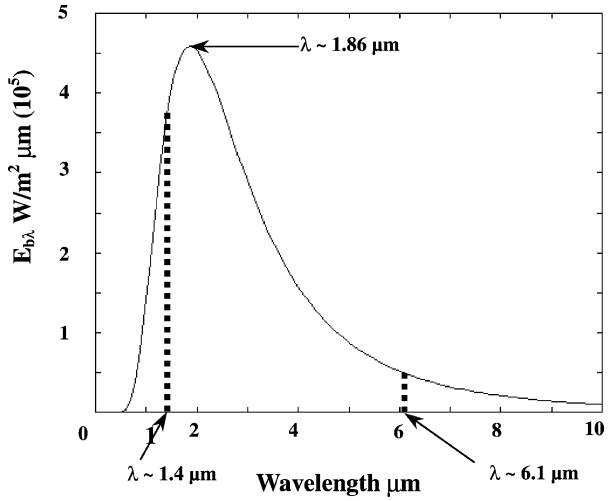

Fig. 2. Spectral black body emissive power for $n = 1.6$, $T = 973$ K, 80% of radiative energy contained within $1.4\,\mu m < \lambda < 6.1\,\mu m$.

emissive power with wavelength for $n = 1.8$ [5] and $T = 973$ K is shown in Fig. 2 and corresponds to SOFC operating conditions. It can be shown that 80% of the radiative emissive power is contained within the infrared spectral region $1.4\,\mu m < \lambda < 6.1\,\mu m$ with the maximum at $\lambda \approx 1.86\,\mu m$.

Fig. 3 shows the radiative properties of YSZ obtained with a 500 μm thick sample. Clearly, a gray body approximation can be used in the radiation modeling of YSZ, as the transmittance is found to be independent of wavelength in the region of interest ($1.4\,\mu m < \lambda < 6.1\,\mu m$). The absorption coefficient of YSZ electrolyte is obtained from

$$Tr = e^{-\kappa L} \quad (2)$$

where Tr is the transmitivity, κ the absorption coefficient and L the thickness of the medium. The optical properties of the cathode are obtained from the imaginary part of dielectric constant spectra [6] and the optical conductivity spectra [7] of $La_{1-x}Sr_xMnO_3$.

The optical thickness ($\tau = \kappa L$) of the fuel cell electrolyte and cathode, based on the dimensions in Table 1, were found

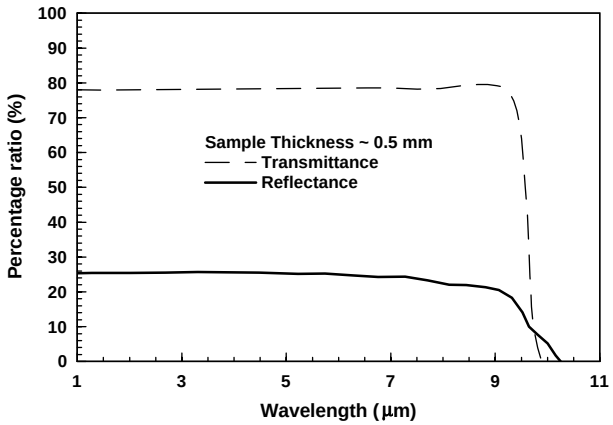

Fig. 3. Optical properties of a 500 μm thick YSZ sample.

Table 1
Monolith fuel cell model description

Region	Type	Dimension (m)
Cathode	Porous ($\phi = 0.3$)	0.0025
Anode	Porous ($\phi = 0.38$)	0.0025
Electrolyte	Solid	0.0005
Current collector	Solid	0.0005

to be 0.25 and 10^4, respectively. The optical properties of the anode material are complicated to calculate as they depend on the distribution of the nickel cermets in YSZ. The presence of Nickel doping makes the anode highly absorbing to thermal radiation, thus resulting in optically thick ($\tau \gg 1$) behavior. Therefore, for lack of experimental data, the absorption coefficient of the anode is assumed to be the same as that of the cathode. Also, the radiation scattering in electrodes is neglected, although this assumption is questionable considering the porous nature of electrodes.

2.2. Radiative model approximation

2.2.1. Rosseland thermal conductivity

For optically thick slabs ($\tau \gg 1$), it has been shown [8] that the radiative heat flux q_R can be estimated with sufficient accuracy through Rosseland approximation as,

$$q_R = -k_R \nabla T \tag{3}$$

where k_R is the radiative conductivity and defined as,

$$k_R = \frac{16 n^2 \sigma T^3}{3\beta_R} \tag{4}$$

In Eq. (4), β_R refers to the Rosseland-mean extinction coefficient, which is equal to the constant absorption coefficient for the gray and non-scattering medium. Unfortunately, the above diffusion approximation is not valid near a boundary, where it often fails quiet miserably [8]. This limitation can be overcome by coupling the diffusion model with the Schuster–Schwartzchild two-flux approximation for locally optically thin regions near the boundaries of the overall optically thick medium.

2.2.2. Schuster–Schwartzchild two-flux approximation

Schuster–Schwartzchild or the two-flux approximation provides a simple solution method for one-dimensional radiation in a thin, plane-parallel slab. In this method, the radiative intensity is assumed to be an isotropic function of the propagation direction, but different, over the upper and lower hemisphere. For a gray, non-scattering medium confined between two isothermal, parallel black plates at temperatures T_{top} and T_{bottom} and separated by a distance L, the two-flux model gives the radiative heat flux as [8]

$$q_R(z) = C_1 e^{2\kappa z} + C_2 e^{-2\kappa z} \tag{5}$$

where

$$C_1 = -\sigma(T_{top}^4 - T^4)e^{-2\kappa L}, \qquad C_2 = \sigma(T_{bottom}^4 - T^4) \tag{6}$$

The radiation transport thus calculated can be coupled with the overall energy conservation by introducing the divergence of the radiative heat flux as a (negative) source term in the energy equation.

Fig. 4 shows a schematic of a two-dimensional enclosure used for validating the Schuster–Schwartzchild radiation model. The bottom and top walls of the enclosure were maintained at constant temperatures of 1000 and 2000 K, respectively, with the sidewalls being adiabatic. Studies were carried out for different optical thickness by varying the absorption coefficient of the enclosed medium.

Fig. 5 shows the temperature variation across the thickness of the liquid medium as predicted by the two-flux approximation, and compares their accuracy with those obtained using the more accurate but computationally intensive DO scheme. Excellent agreement in temperature predictions is seen for extremely optically thin materials. Large deviations are observed with increase in optical thickness with the Schuster–Schwartzchild approximation failing for optical thickness greater than one.

2.3. Fuel cell model

A general-purpose computational fluid dynamics software (FLUENT^{TM}) was used for modeling the transport and heat transfer phenomena occurring within the fuel cell [9]. The Navier–Stokes and transport equations are solved to obtain the flow, species concentrations and temperature at each location in the cell. A coupled electrochemical model calculates the current density, cell voltage, and heat flux at the electrodes based on the species and temperature distribution within the cell. This information is then passed back to CFD model, where it is used to update the species and temperature fields. The process continues in an iterative manner until convergence is reached.

The single-cell model (Fig. 1) represents a repeating unit cell in the center of a large stack. Hence, adiabatic boundary conditions were assumed on all cell walls. Four chemical species, namely H_2, O_2, H_2O and N_2, were tracked in

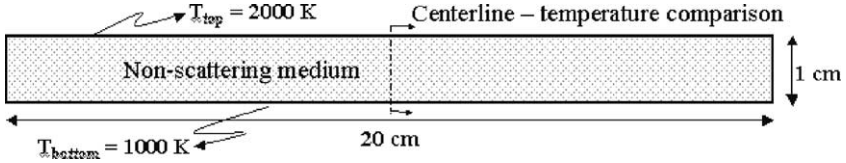

Fig. 4. Schematic of two-dimensional model in FLUENT^{TM} used for validation of Schuster–Schwartzchild two-flux radiation model.

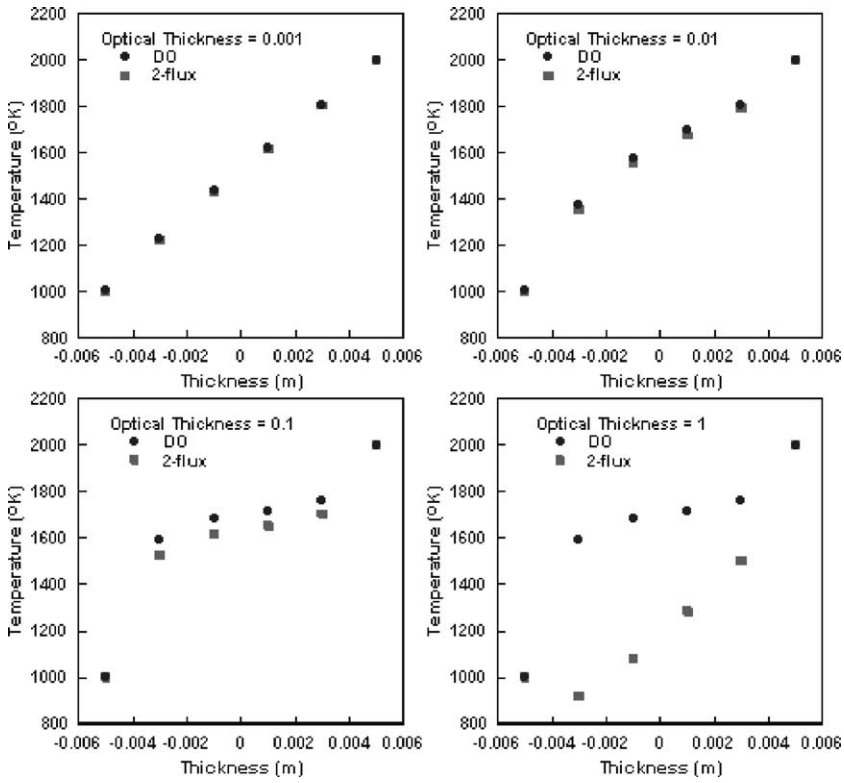

Fig. 5. Comparison of two-flux method and more accurate discrete ordinate (DO) scheme for different optical thickness. The two-flux method fails for optical thickness greater than unity.

the simulation. The inlet flows of air and fuel were specified using constant mass flow boundary conditions. Air was delivered to the cathode at 0.32 mg/s and 750 K. The fuel mass flow rate was 0.0045 mg/s at 750 K with the composition of fuel by mass fraction being 78% H_2 and 28% H_2O. A fixed pressure condition was used for the fuel and air outlets. The pressure drops in the porous cathode and anode regions were modeled using Darcy's law, and the transport of the reactant species to the electrolyte/anode interface was modeled through diffusion of a multi-component mixture through porous electrodes.

The air and fuel streams were modeled as ideal gas mixtures with the gas viscosities and thermal conductivities calculated based on kinetic theory. The material properties of the solids used in the calculations are listed in Table 2. The anode and cathode regions were modeled as porous media with porosities of 0.38 and 0.30, respectively. The material properties of the porous medium were computed as the volume average of the fluid and solid properties. The three dimensional simulations of the unit cell, including the internal gas flow channels, were performed using a fine mesh of 37,440 computational elements.

Table 2
Solid material properties

Material	Density (kg/m^3)	Thermal conductivity (W/(m K))
Anode-solid	3030	5.84
Cathode-solid	3310	1.86
Electrolyte	5160	2.16
Current collector	8030	0.1

3. Results

3.1. Radiation effect

Fig. 6 shows the temperature variation along the cathode-electrolyte and anode-electrolyte walls of the fuel cell with and without inclusion of radiation effects. Clearly, the heat transfer enhancement due to radiation results in overall decrease of the temperature level within the cell, as well as the less steep temperature gradients along the cell.

The maximum electrical work obtainable in a fuel cell, operating at constant temperature and pressure, is given by the change in Gibb's free energy (ΔG) of the electrochemical reaction. The relationship between the Gibb's free energy (G) and the reaction enthalpy (H) is known to be [10],

$$\Delta G = \Delta H - T\,\Delta S \tag{7}$$

where ΔH corresponds to the total thermal energy available in the system, ΔS denotes the change in entropy and $T\,\Delta S$ represents the amount of heat generated by a fuel cell operating reversibly. The change in entropy (ΔS) is a non-linear

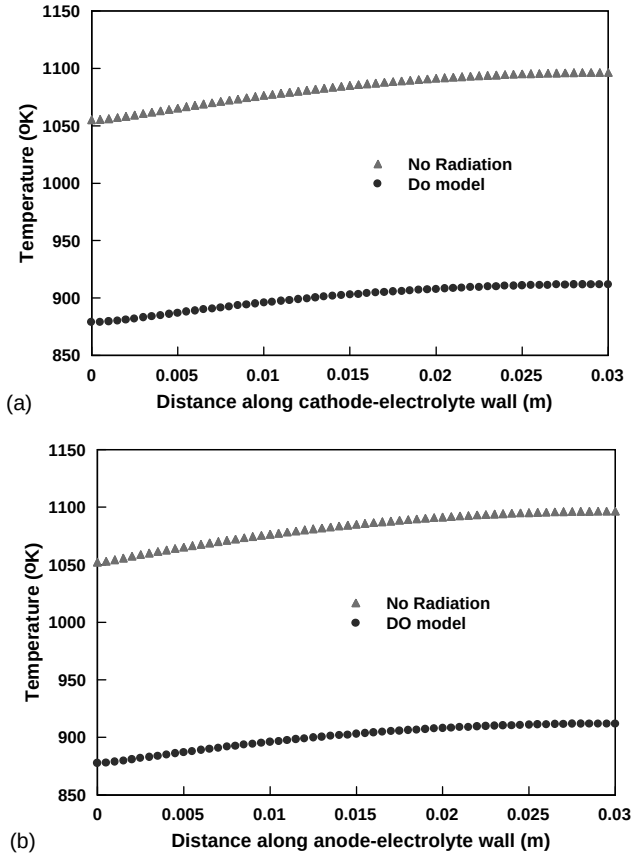

Fig. 6. Temperature along a centerline passing through the length of the fuel cell (x-direction) on (a) cathode-electrolyte and (b) anode-electrolyte walls with and without accounting for radiation heat transfer.

function of temperature and is of the form,

$$\Delta S = \Delta S^0 + a \ln\left(\frac{T}{298}\right) + b(T - 298) + \frac{1}{2}c(T - 298)^2 \tag{8}$$

where a, b, and c are empirical constants [10] and ΔS^0 is the standard entropy of formation at 298 K.

The additional heat transfer path provided by radiation results in a fairly uniform temperature field within the fuel cell system with reduction in the maximum temperatures. Inclusion of radiation effects resulted in a 20% drop in the $T\,\Delta S$ value, thereby, accounting for the 180 K decrease in the fuel cell temperature. Also, the maximum available electrical work, as given in Eq. (7), increases with decrease in $T\,\Delta S$ and results in corresponding higher fuel cell voltage. Indeed, the observed 180 K drop in the cell temperature (Fig. 6) causes a corresponding increase in the Gibbs free energy, and results in a significant increase in the cell voltage from 0.65 to 0.74 V.

3.2. Rosseland/two-flux model

Although the DO method is very accurate in accounting for absorption and emission of thermal radiation through the solution of the RTE, the computational costs involved along with the memory requirements make the implementation prohibitive for extensive design calculations and optimization. To overcome the above problem, a simplified radiation model has been developed that takes advantage of the differences in optical properties of the fuel cell materials to reduce the computational expense. In this approach, radiative heat transfer in the optically thin electrolyte was modeled using the Schuster–Schwartzchild model, whereas radiation in the optically thick electrodes was accounted through the Rosseland diffusion approximation. Failure of the diffusion model near the boundaries was overcome by employing a very fine grid near the boundaries. Subsequently, the first few cells along the boundary walls of the electrode were treated as optically thin medium and solved using the two-flux approximation method as well.

Fig. 7 shows the variation of temperature, along the length of the anode-electrolyte interface (x-direction) and across the thickness of the fuel cell (at the location $x = 0.025$ m), for the different radiation models. The maximum difference in the temperature predictions obtained using a highly accurate discrete ordinate (DO) method was found to be <10 K as compared to the simplified Rosseland/two-flux approximate

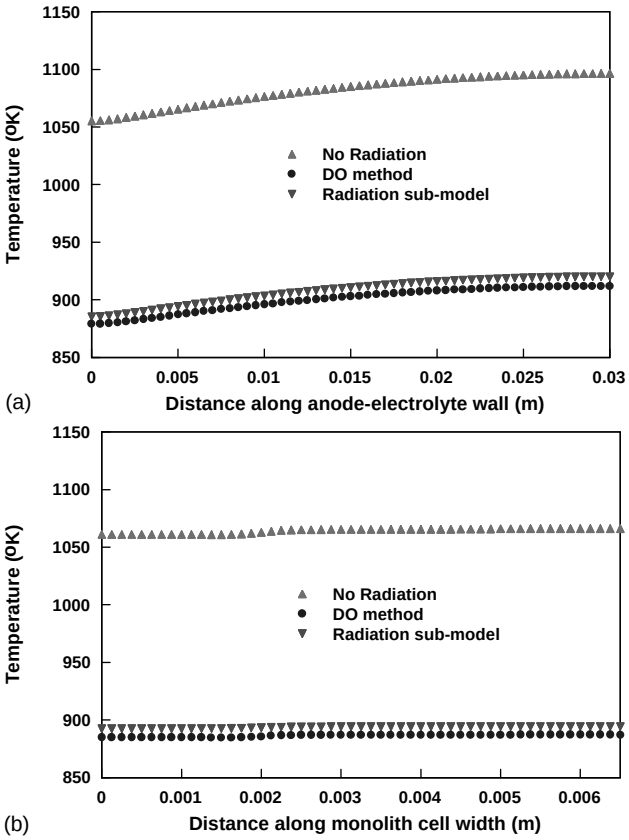

Fig. 7. Validation of Rosseland/two-flux radiation sub-model through temperature comparison with DO predictions along (a) centerline passing along the anode-electrolyte interface and (b) thickness of the fuel cell (at axial position $x = 0.025$ m).

scheme. At the same time, the latter radiation sub-model resulted in almost a ten-fold reduction of the CPU time from 658 min for the DO method to only 76 min with the simplified Rosseland/two-flux approximation scheme.

4. Conclusions

Based on the rigorous analysis of radiation heat transfer in a single unit SOFC, the following conclusions can be drawn:

(i) Though commonly neglected, radiation heat transfer effects are significant and need to be accounted for accurate prediction of the temperature field and the fuel cell output voltage.
(ii) The computationally expensive discrete ordinate method can be replaced by a simplified radiation sub-model, which is based on Rosseland diffusion approximation for the optically thick electrodes and the Schuster–Schwartzchild two-flux method for the optically thin electrolyte.
(iii) Significant saving in computational time is achieved with the Rosseland/two-flux radiation model without much loss in accuracy in the temperature/voltage predictions when compared to the discrete ordinate (DO) method.

Acknowledgements

The US Department of Energy's National Energy Technology Laboratory (NETL) funded the work summarized in this paper as part of the Solid-State Energy Conversion Alliance (SECA) Core Technology program.

References

[1] T.Q. Minh, T. Takahashi, Science and Technology of Ceramic Fuel Cells, Elsevier, New York, 1995.
[2] K.P. Recknagle, R.E. Williford, L.A. Chick, M.A. Rector, M.A. Khaleel, Three-dimensional thermo-fluid electrochemical modeling of planar SOFC stack, J. Power Sources 113 (2003) 109–114.
[3] H. Yakabe, T. Ogiwara, I. Yasuda, M. Hishunuma, Three-dimensional model calculation for planar SOFC, J. Power Sources 102 (2001) 144–154.
[4] J. Hartvigsen, S. Elangovan, A. Khandkar, Modeling, Design and Performance of Solid Oxide Fuel Cells, vol. 105, Zirconia V, 2002.
[5] X. L. Ruan, M. Kaviany, Dependent Scattering and Field Enhancement in Monochromatic Irradiated Random Porous Media, in: Proceedings of the ASME Summer Heat Transfer Conference, HT2003-47233, Las Vegas, July 2003.
[6] Y. Okimoto, T. Katsufuji, T. Ishikawa, T. Arima, Y. Tokura, Variation of electronic structure in $La_{1-x}Sr_xMnO_3$ ($0 < x < 0.3$) as investigated by optical conductivity spectra, Phys. Rev. B 55 (1997) 4206–4214.
[7] Y. Okimoto, T. Katsufuji, A. Urushibara, T. Arima, Y. Tokura, Anomalous variation of optical spectra with spin polarization in double-exchange ferromagnet, Phys. Rev. 75 (1995) 109–112.
[8] M.F. Modest, Radiative Heat Transfer, McGraw-Hill, New York, 1993.
[9] M. Prinkey, R. Gemmen, W. Rogers, Application of a new CFD analysis tool for SOFC technology, in: Proceedings of the ASME IMECE Conference, November 2001, New York.
[10] J.H. Hirschenhofer, D.B. Stauffer, R.R. Engleman, M.G. Klett, Fuel Cell Handbook, fourth ed., Department of Energy, Fossil Energy Technology Centre, 1998.